JBC RESEARCH ARTICLE

Exploiting the distinctive properties of the bacterial and human MutS homolog sliding clamps on mismatched DNA

Received for publication, October 22, 2021, and in revised form, September 13, 2022 Published, Papers in Press, September 17, 2022,
https://doi.org/10.1016/j.jbc.2022.102505

Brooke M. Britton[1], James A. London[1], Juana Martin-Lopez[1], Nathan D. Jones[1], Jiaquan Liu[1], Jong-Bong Lee[2,3], and Richard Fishel[1,*]

From the [1]Department of Cancer Biology and Genetics, The Ohio State University Wexner Medical Center, Columbus, Ohio, USA; [2]Department of Physics, Pohang University of Science and Technology (POSTECH), Pohang, Korea; [3]Interdisciplinary Bioscience and Bioengineering, POSTECH, Pohang, Korea

Edited by Patrick Sung

MutS homologs (MSHs) are highly conserved core components of DNA mismatch repair. Mismatch recognition provokes ATP-binding by MSH proteins that drives a conformational transition from a short-lived lesion-searching clamp to an extremely stable sliding clamp on the DNA. Here, we have expanded on previous bulk biochemical studies to examine the stability, lifetime, and kinetics of bacterial and human MSH sliding clamps on mismatched DNA using surface plasmon resonance and single-molecule analysis of fluorescently labeled proteins. We found that ATP-bound MSH complexes bound to blocked-end or very long mismatched DNAs were extremely stable over a range of ionic conditions. These observations underpinned the development of a high-throughput Förster resonance energy transfer system that specifically detects the formation of MSH sliding clamps on mismatched DNA. The Förster resonance energy transfer system is capable of distinguishing between HsMSH2-HsMSH3 and HsMSH2-HsMSH6 and appears suitable for chemical inhibitor screens. Taken together, our results provide additional insight into MSH sliding clamps as well as methods to distinguish their functions in mismatch repair.

Mismatch repair (MMR) corrects polymerase misincorporation errors, selected chemical and/or physical DNA damage as well as sequence heterology resulting from DNA recombination (1). Homologs of the prototypical *E.coli* (Ec) EcMutS and EcMutL are the most highly conserved MMR components across biology. The function(s) of the MutS homologs (MSHs) and MutL homologs (MLHs/PMS) have been of interest for decades. It is well known that MSH proteins recognize mismatched nucleotides (2, 3). However, the operation of these essential components following mismatch recognition has not been definitively established (1–6).

MSH proteins function as dimers or heterodimers with each half containing a highly conserved Walker A/B nucleotide-binding motif (7). In addition to simple nucleotide mismatches, MSH proteins recognize insertion-deletion loop-type (IDL) mismatches, and several relatives have evolved to recognize recombination cross-over structures during meiosis (8–10). The MSH search and recognition process has been shown to involve the formation of an incipient clamp that interrogates the DNA by rotation-coupled diffusion (11, 12). ATP binding by all MSH proteins results in the formation of a stable freely diffusing sliding clamp on the DNA (9, 10, 12–23). The biochemical function of the MLH/PMS proteins had been largely enigmatic until recent single-molecule imaging studies showed that the EcMutS sliding clamp provides a platform for EcMutL to form a second extremely stable sliding clamp on DNA containing a mismatch (13, 24–28). In *E. coli*, the MutL sliding clamp then functions to enhance EcMutH DNA association and GATC-hemimethylation incision activity (27, 29, 30) as well as EcUvrD strand-specific unwinding-displacement activity (27). The human HsMSH2-HsMSH6 and HsMLH1-HsPMS2 similarly form a cascade of sliding clamps (28), while the yeast homologs clearly interact on mismatched DNA with the sliding clamp details under investigation (23, 31–33).

Mutation of HsMSH2, HsMSH6, HsMLH1, and HsPMS2 cause the most common cancer predisposition in humans known as Lynch syndrome or hereditary nonpolyposis colorectal cancer (LS/HNPCC) (1, 34–38). This observation is consistent with a pathogenic dysfunction of the major HsMSH2-HsMSH6 or HsMLH1-HsPMS2 heterodimers (20, 39–41). Most cells that contain these major human heterodimers also possess the HsMSH2-HsMSH3 heterodimer (8, 10, 42). HsMSH2-HsMSH6 recognizes a broad array of common replication errors that included single nucleotide and small IDL mismatches, while HsMSH2-HsMSH3 recognizes some single nucleotide mismatches and larger IDL (1–14 nucleotides) mismatches (8, 10, 43). Mutations of HsMSH3 have not been found to cause LS/HNPCC (44–46). However, mutation of HsMSH3 appears to eliminate the pathogenic expansion of trinucleotide repeat (TNR) disease genes such as Huntington's disease and myotonic dystrophy (47). Together, these observations suggest that hampering HsMSH2-HsMSH3 activity, without affecting HsMSH2-HsMSH6 functions, might engender a useful therapeutic for TNR disease pathologies while not encouraging cancer.

Here, we have employed a variety of bulk and high-resolution biophysical methods to dissect MSH progression

* For correspondence: Richard Fishel, fishel.7@osu.edu.

to a stable sliding clamp. We found bacterial MutS mismatch affinity continued to increase with decreasing ionic strength, while HsMSH2-HsMSH6 mismatch affinity peaked at a total ionic strength of ∼100 mM (13, 48, 49). The dissociation kinetics and lifetime of the ATP-bound MSH sliding clamp determined by surface plasmon resonance (SPR) analysis and single-molecule total internal reflection fluorescence (smTIRF) microscopy, respectively, was unaffected over a wide range of ionic conditions. The extremely stable sliding clamp formed by MSH proteins on end-blocked DNA suggested that a Förster resonance energy transfer (FRET) system could be developed that was capable of clearly distinguishing HsMSH2-HsMSH3 and HsMSH2-HsMSH6 functions. We show that Cy5-labeled HsMSH2-HsMSH3 uniquely forms sliding clamps with a Cy3-labeled blocked-end $(CA)_4$ lDL producing a strong time-averaged FRET signal. In contrast, Cy3-labeled HsMSH2-HsMHS6 appears more promiscuous but forms sliding clamps and time-averaged FRET more efficiently with Cy3-labeled DNA containing a G/T mismatch compared to the Cy3-labeled $(CA)_4$ IDL. This FRET system is extremely durable and can tolerate room temperature manipulations and dimethyl sulfoxide (DMSO) concentrations below 0.5%, a common solvent in high-throughput (HTP) large-scale compound screens.

Results

Ionic dependence of mismatch binding and ATP-induced dissociation

MSH proteins preferentially bind DNA containing mismatched nucleotides (3, 8, 10, 15, 49–51). Previous studies showed that binding to both a mismatched and fully duplex DNA increased with decreasing ionic strength (13, 48, 49). Kinetic analysis of MSH-mismatch binding has been examined by SPR, resulting in equilibrium binding dissociation constants (K_D) that appeared generally similar to electrophoretic mobility shift analysis (3, 13, 20, 23, 52).

To eliminate unlinked biochemical issues, we examined the EcMutS(D835R,R840E) protein that is incapable of tetramerization but fully functional for mismatch repair (hereafter referred to as EcMutS) (53). We utilized SPR to determine the K_D for EcMutS (11.5 ± 0.1 nM and 13.0 ± 0.1 nM) and HsMSH2-HsMSH6 (1.01 ± 0.02 nM and 1.09 ± 0.02 nM) on open-end *versus* blocked-end mismatched DNA, respectively (Figs. S1 and S2). These results confirm previous studies that demonstrated MSH binding to a mismatched was largely unaffected by whether the DNA end was open or blocked by a biotin–streptavidin linkage (13, 16).

The salt-dependent binding of EcMutS and HsMSH2-HsMSH6 to open-end and blocked-end mismatched DNA was then examined by SPR at a single intermediate MSH concentration that corresponded to ∼80% saturation (Fig. 1; Tables 1 and S2; Experimental procedures). We found that the apparent K_d for EcMutS decreased exponentially over a wide range NaCl concentrations (Fig. 1*A*). These observations appeared qualitatively similar to previous studies (54). In contrast, we found HsMSH2-HsMSH6 was most avidly bound to the mismatched DNA at ∼75 mM NaCl (Fig. 1*B*), which appears significantly different than previous electrophoretic mobility shift analysis (48). Whether the DNA contained open-ends or biotin–streptavidin blocked-ends did not dramatically influence mismatch binding affinity for either EcMutS or HsMSH2-HsMSH6 (Fig. 1).

The k_{off} of EcMutS and HsMSH2-HsMSH6 did not vary significantly over the range of salt concentrations with open-end or blocked-end mismatched DNA (Tables 1 and S2). However, in the presence of ATP, the $k_{off•ATP}$ for EcMutS and HsMSH2-HsMSH6 on open-ended mismatched DNA increased 200-fold to 2000-fold (Tables 1 and S2), while the $k_{off•ATP}$ on blocked-end decreased slightly compared to the k_{off} in the absence of ATP (Table 1 and S2). These results are consistent with historical studies that demonstrated MSH proteins such as EcMutS and HsMSH2-HsMSH6 form sliding clamps in the presence of ATP, which rapidly dissociate from the mismatch or lesion but are retained on the DNA when the ends are blocked by biotin–streptavidin (9, 10, 12–14, 16, 17, 19, 21–23, 52, 54, 55). We note that the salt concentration did not substantially influence the $k_{off•ATP}$ on both open-end and blocked-end mismatched DNA (Tables 1 and S2).

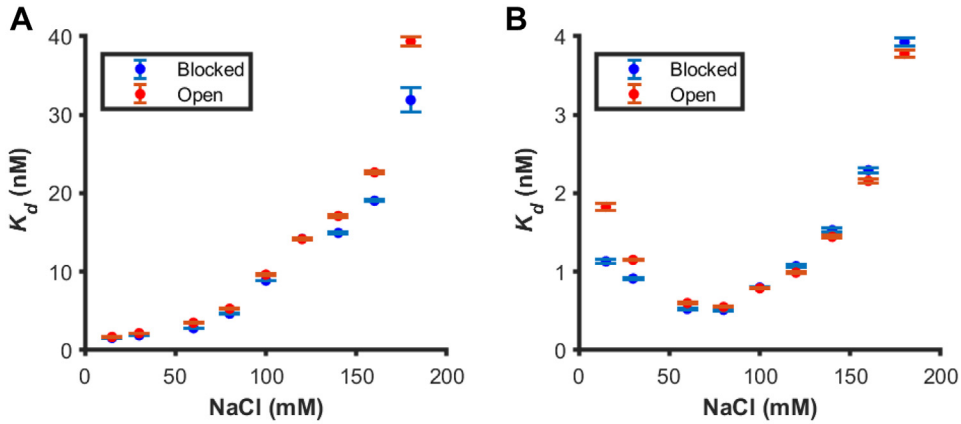

Figure 1. Binding affinity of EcMutS and HsMSH2-HsMSH6. Surface plasmon resonance association rates. The apparent equilibrium dissociation constant (K_d) for (*A*) EcMutS (40 nM) and (*B*) HsMSH2-HsMSH6 (40 nM) in the absence of ATP across a wide range of salt concentrations. Standard error of each constant, estimated from the fitted model, are shown but are ∼1/100 the mean constants' values.

Table 1
Dissociation kinetics of EcMutS

	Open-end DNA		Blocked-end DNA	
NaCl (mM)	k_{off}[a] (s^{-1}) × 10^{-3}	$k_{off•ATP}$[b] (s^{-1}) × 10^{-3}	k_{off}[a] (s^{-1}) × 10^{-3}	$k_{off•ATP}$[b] (s^{-1}) × 10^{-3}
15	1.49 (0.007)	348 (4.35)	1.02 (0.008)	0.54 (0.014)
30	2.09 (0.009)	240 (4.79)	1.29 (0.007)	0.54 (0.013)
60	2.54 (0.010)	445 (10.2)	1.63 (0.009)	0.52 (0.016)
80	2.87 (0.012)	349 (10.5)	2.31 (0.007)	0.80 (0.014)
100	3.22 (0.010)	270 (8.26)	2.70 (0.006)	1.06 (0.012)
120	3.35 (0.011)	306 (10.7)	2.97 (0.009)	1.53 (0.019)
140	1.49 (0.007)	330 (11.0)	3.17 (0.011)	1.56 (0.024)
160	2.09 (0.009)	203 (6.20)	3.40 (0.012)	1.68 (0.026)
180	2.54 (0.010)	110 (4.98)	3.56 (0.028)	1.97 (0.066)

Surface plasmon resonance dissociation studies. First-order rate constants of EcMutS (40 nM) in the absence (k_{off}) and presence of ATP (1 mM, $k_{off•ATP}$). Open-end DNA (left) and blocked-end DNA (right) show similar rates of dissociation in the absence of ATP (k_{off}). EcMutS sliding clamps quickly slide off open-end DNA (left) but are retained for longer on blocked-end DNAs (right).
[a] First-order rate constants in the absence of ATP (1 mM). Standard error in parentheses.
[b] First-order rate constants in the presence of ATP (1 mM). Standard error in parentheses.

ATP-bound MSH sliding clamps are extremely stable on mismatched DNA

smTIRF was used to probe the stability of Alexa647-labeled EcMutS sliding clamps on mismatched DNA (Fig. 2). In this system, the trajectory, diffusion dynamics, and lifetime of single EcMutS sliding clamps were determined over a range of ionic strengths. Numerous single particles could be easily resolved on the mismatched DNA (Figs. 2*A* and S3), and the trajectories binned to determine the diffusion coefficient as well as the lifetime as previously described (12, 14, 26, 27). We found that the diffusion coefficient increased with increasing ionic strength (Fig. 2*B*). These observations are consistent with previous studies of *Thermus aquaticus* (Taq) TaqMutS and suggest that EcMutS ATP-bound sliding clamps undergo thermal diffusion along the DNA while maintaining intermittent contact with the backbone (14). In contrast, the lifetime appeared relatively constant (195 ± 11 s), suggesting that EcMutS sliding clamps remain stably linked to the mismatched DNA over a wide range of ionic strength (Figs. 2*C* and S4).

We similarly examine the lifetime of Cy3-labeled HsMSH2-HsMSH3 and HsMSH2-HsMSH6 sliding clamps on DNA by smTIRF (Fig. 2, *D* and *E*, Experimental procedures). For these studies, we used a G/T mismatch as the preferred substrate for HsMSH2-HsMSH6 and a CAG IDL mismatch as the preferred substrate for HsMSH2-HsMSH3. While the lifetime of HsMSH2-HsMSH6 sliding clamps on DNA was similar to EcMutS (163 ± 40 s; Fig. 2*D*), the lifetime of HsMSH2-HsMSH3 was almost six times longer (1315 ± 389 s; Fig. 2*E*). Other than the IDL substrate preferences identified more than 2 decades ago (8, 10, 42, 56), this is the first indication that HsMSH2-HsMSH3 may behave significantly different as a sliding clamp on the DNA compared to the major MSH proteins that function in postreplication MMR.

A FRET-based system that distinguishes human MSH sliding clamps

The stability of MSH sliding clamps on a mismatched DNA suggested that a bulk FRET scheme might rapidly distinguish mismatch bound and sliding clamp forms of the human MSH heterodimer proteins. This system is based on previous smTIRF studies that determined the binding and sliding clamp kinetics of the *Thermus Aquaticus* MutS (TaqMutS) (12). We designed a 41-mer oligonucleotide containing either no mismatch, a G/T mismatch, or a $(CA)_4$ IDL with a biotin on both ends (Fig. 3*A*). These oligonucleotides were additionally labeled with Cy5 at a thymine nucleotide nine base pairs from the mismatch (Fig. 3*A*). Previous studies with TaqMutS suggested that mispair-specific binding will place the Cy3-MSH in close proximity to the Cy5-DNA resulting in FRET (12). Because the Cy3-label is located on the N terminus of HsMSH2 in the HsMSH2-HsMSH6 heterodimer and the N terminus of HsMSH3 in the HsMSH2-HsMSH3 heterodimer, we expect a lower FRET efficiency than with the TaqMutS where the label was located on the clasp arm significantly closer to the Cy5-DNA label (12). In the presence of ATP, both HsMSH2-HsMSH3 and HsMSH2-HsMSH6 will form a sliding clamp (10, 16, 23, 52). Including the glycosylation-free avidin derivative neutravidin that binds tightly to the biotin ends of the DNA substrates retains these sliding clamps on the DNA, where they freely diffuse along the length between the ends (Fig. 3*A*). We calculate that these sliding clamps may transit the length of this relatively short DNA 100s of times per second, resulting in a time-averaged FRET with a lower efficiency than when stably bound to the mismatch (12).

A fixed concentration of HsMSH2-HsMSH6 (20 nM) was examined in the presence of a 1:2 and 1:4 M ratio of Cy5-labeled DNA (Fig. 3, *B* and *C*). As a control, we found that HsMSH2-HsMSH6 only transiently interacts with the G/C duplex DNA, resulting in little or no FRET (Fig. 3, *B–E*). In contrast, HsMSH2-HsMSH6 specifically binds to the oligonucleotide containing a G/T mismatch resulting in a statistically significant elevated FRET (Fig. 3, *B–E*; G/C, black bar *versus* G/T red bar, $p_{40\ nM} = 0.0006$, $p_{80\ nM} = 0.0004$; ***). As predicted, the addition of ATP resulted in a FRET reduction at both DNA concentrations (Fig. 3, *B–E*; G/T red bar *versus* G/T_{ATP} green bar, $p_{40\ nM} = 0.005$, $p_{80\ nM} = 0.03$), which remained significantly above the G/C background control (Fig. 3, *B–E*; G/C black bar *versus* G/T_{ATP} green bar, $p_{40\ nM} = 0.0007$, $p_{80\ nM} = 0.002$). We noted a slight reduction in the

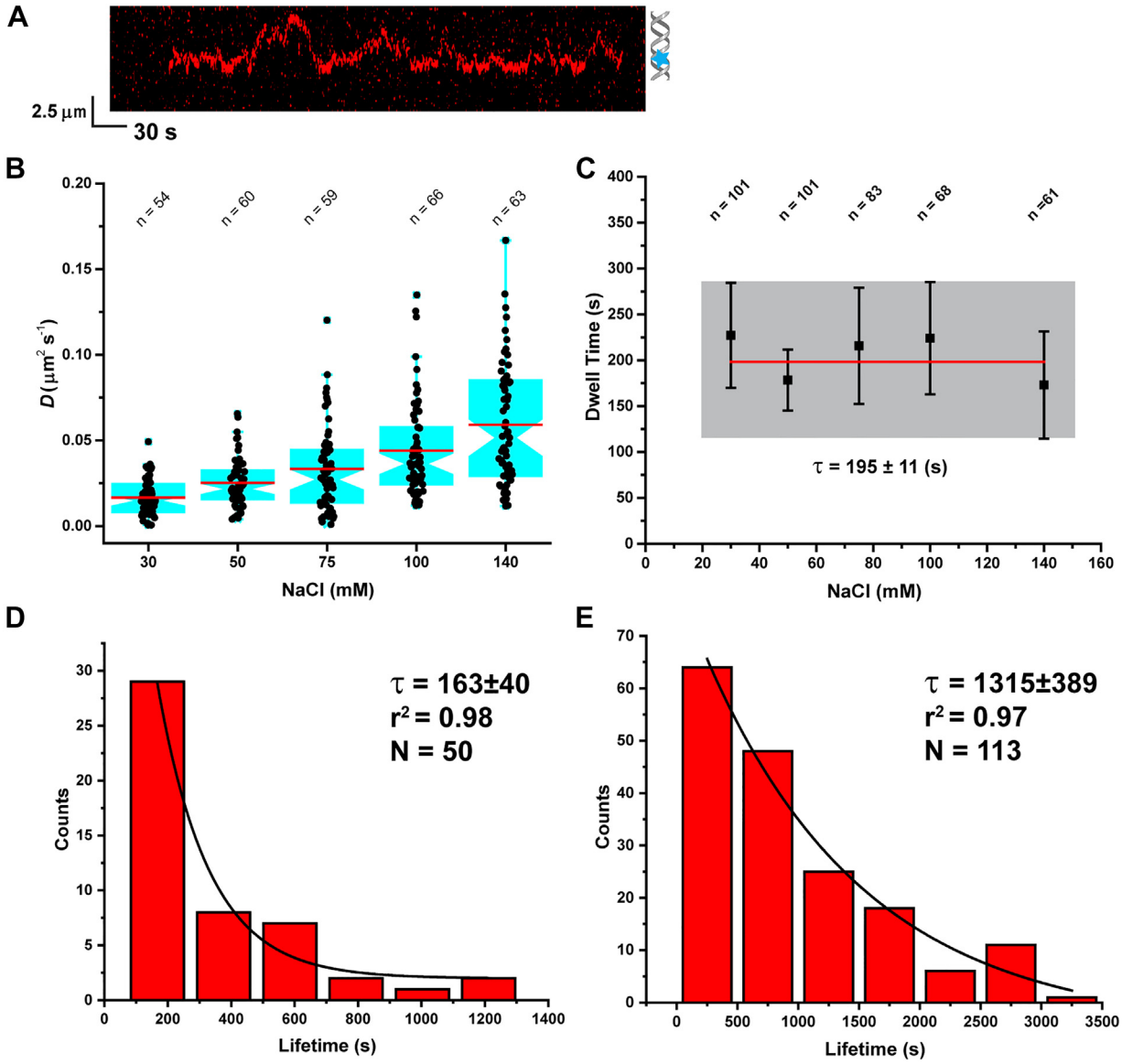

Figure 2. MSH lifetimes. Single-molecule analysis of individual labeled MSH sliding clamps. *A*, representative kymograph of a single EcMutS diffusion event at 100 mM NaCl. *Blue star* indicates the mismatch position. Scale bar indicates kymograph length (time) and spatial position. *B*, box plots of diffusion for EcMutS (5 nM) sliding clamps in the presence of ATP (1 mM) across a wide range of ionic strengths. *Red line* represents the mean and *indent* represents median. EcMutS sliding clamp diffusion rate increases with increasing NaCl concentration suggesting intermittent contact with the DNA backbone. *C*, the lifetime of EcMutS (5 nM) sliding clamps in the presence of ATP (1 mM) across a wide range of ionic strength conditions. *Black square* represents average value and *whiskers* represent standard deviation. *Red line* represents the mean of all dwell times. *Gray box* outlines width of one standard deviation of all the dwell times to highlight the similarity of the spread. Average lifetime was found to be 195 ± 11 s. *D*, histogram represents lifetime distributions of binned HsMSH2-HsMSH6 (1 nM) sliding clamps in the presence of ATP (1 mM) at 100 mM NaCl. Data were fit to a single exponential decay to derive average lifetime (mean ± s.e.; n = number of events). Average lifetime was found to be 163 ± 40 s.e., histogram represents lifetime distributions of binned HsMSH2-HsMSH3 (0.5 nM) sliding clamps in the presence of ATP (1 mM) at 100 mM KGlu. Data were fit to a single exponential decay to derive average lifetime (mean ± s.e.; n = number of events). Average lifetime was found to be 1315 ± 389 s. Multiple laser power settings were examined to clearly distinguish protein dissociation from fluorophore photobleaching. MSH, MutS homolog.

G/T-binding FRET efficiency of HsMSH2-HsMSH6 with increased DNA concentration that could be due to an increased background of direct Cy5 excitation by the 532 nm laser.

The *Saccharomyces cerevisiae* (Sc) ScMSH2-ScMSH6 heterodimer is known to recognize small IDLs in addition to single nucleotide mismatches (17, 33, 51, 57). We found that incubation of the 8 bp $(CA)_4$ IDL with HsMSH2-HsMSH6 resulted in significant FRET above the G/C control (Fig. 3, *B–E*) that decreased in the presence of ATP consistent with the formation of a sliding clamp (Fig. 3, *B–E*). In all cases, the FRET efficiency was reduced compared to G/T mismatch binding in the absence of ATP (Fig. 3, *B–E*). These observations are consistent with the conclusion that Cy3-labeled HsMSH2-HsMSH6 binds and forms an ATP-bound sliding clamp on Cy5-labeled mismatched DNA generating a strong and reproducible time-averaged FRET. However, the FRET distinction between HsMSH2-HsMSH6 binding to a $(CA)_4$

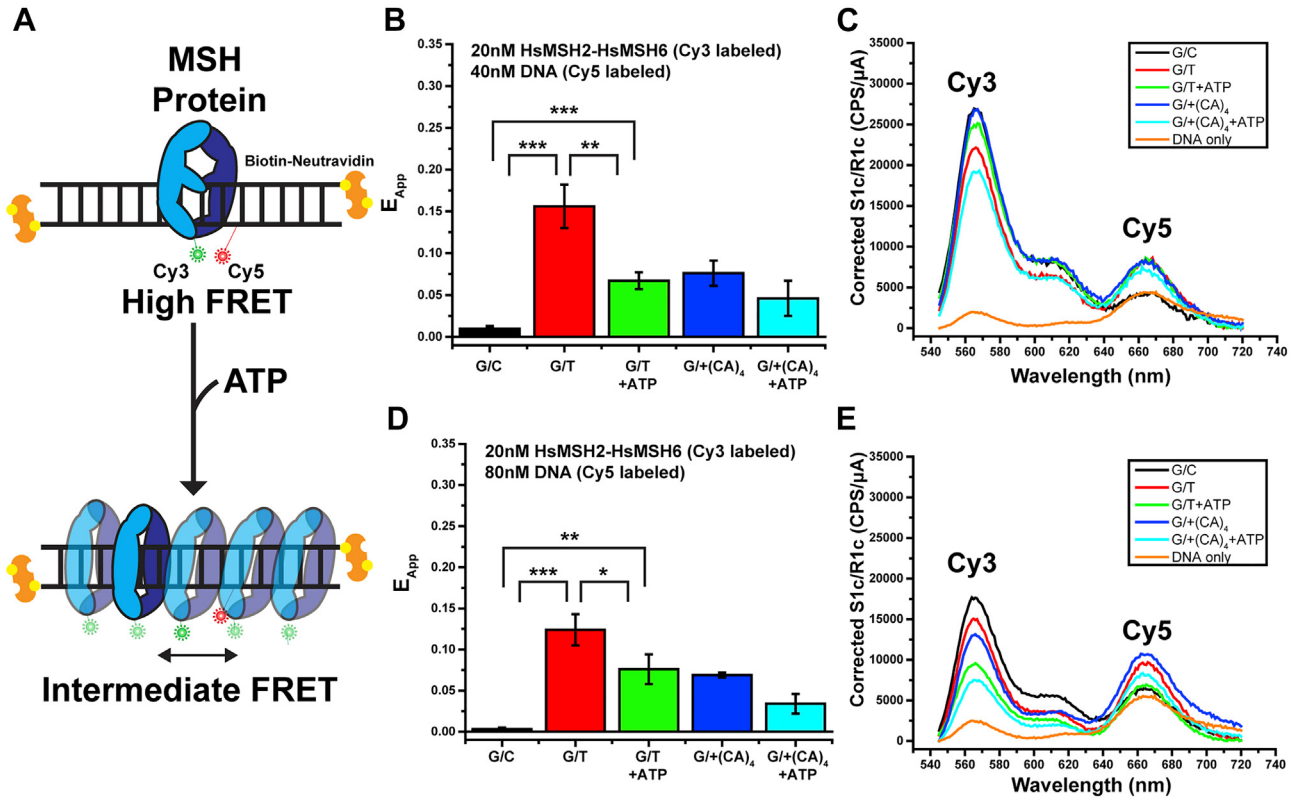

Figure 3. A FRET-based assay for distinguishing HsMSH2-HsMSH6 and HsMSH2-HsMSH3 activities. *A*, the assay utilizes a short DNA oligo with double blocked-ends. These biotin-neutravidin linkages will trap MSH clamps on the DNA and prevent dissociation from the end. A FRET acceptor (Cy5) has been placed on the DNA near the mismatch. A FRET donor (Cy3) has been placed on the protein of interest. MSH protein binding to a mismatch result in a high FRET state (*top*). Upon the addition of ATP, the MSH clamps will transition into stable sliding clamps that diffuse along the DNA. This conformation of the protein results in an intermediate or time averaged FRET (*bottom*). *B*, E_{App} bar graph of 1:4 (HsMSH2-HsMSH6:DNA) for G/C; G/T; G/T + ATP;G/+$(CA)_4$; G/+$(CA)_4$ + ATP (mean ± SD). HsMSH2-HsMSH6 does not bind G/C DNA (*black*) and preferentially binds G/T DNA (*red*). HsMSH2-HsMSH6 displays a reduced FRET efficiency upon binding ATP. $^{**}p < 0.01$;$^{***}p < 0.001$; by unpaired *t* test. *C*, representative intensity *versus* wavelength of 1:4 (HsMSH2-HsMSH6:DNA) for G/C; G/T; G/T + ATP; G/+$(CA)_4$; G/+$(CA)_4$ + ATP. *D*, E_{App} bar graph of 1:2 (HsMSH2-HsMSH6:DNA) for G/C; G/T; G/T + ATP; G/+$(CA)_4$; G/+$(CA)_4$ + ATP (mean ± SD). HsMSH2-HsMSH6 does not bind G/C DNA (*black*) and preferentially binds G/T DNA (*red*). HsMSH2-HsMSH6 displays a reduced FRET efficiency upon binding ATP. $^{*}p < 0.05$; $^{**}p < 0.01$; $^{***}p < 0.001$; by unpaired *t* test. *E*, representative intensity *versus* wavelength of 1:2 (HsMSH2-HsMSH6:DNA) for G/C; G/T; G/T + ATP; G/+$(CA)_4$; G/+$(CA)_4$ + ATP. FRET, Förster resonance energy transfer; MSH, MutS homolog.

mismatched DNA and the formation of a sliding clamp on either a G/T or $(CA)_4$ mismatch is limited (Fig. 3, *B–E*).

We found that incubation of Cy3-labeled HsMSH2-HsMSH3 with the G/T mismatched DNA did not result in any FRET above the control G/C duplex DNA (Fig. 4, *A–D*). These observations suggest the HsMSH2-HsMSH3 is largely incapable of recognizing or forming sliding clamp in the presence of a G/T mismatch (33). However, a strong FRET was observed in the presence of the $(CA)_4$ IDL mismatched oligonucleotide that resolved to a lower time-averaged FRET in the presence of ATP (Fig. 4, *A–D*). Compared to HsMSH2-HsMSH6, the distinction between G/T and $(CA)_4$ IDL is significant. Moreover, the room temperature stability of HsMSH2-HsMSH3, where the smTIRF studies were performed, suggest that this FRET-based system might be a useful screening tool for potential inhibitory compounds.

DMSO affects the FRET efficiency but is correctable

Most chemical compound libraries are dissolved in DMSO, a polar aprotic solvent capable of solubilizing polar and nonpolar compounds that is also miscible in water (58, 59). We examine the effect of DMSO on the protein and DNA fluorophore environment (Fig. 5). An intrinsic fluorescence increase was observed around the FRET emission wavelengths (650–750 nm; Fig. 5*A*). Moreover, 5% DMSO significantly reduced the direct excitation and FRET excitation peaks when included with Cy3-labeled HsMSH2-HsMSH6 and Cy5-labeled G/T mismatched DNA (Fig. 5*B*). The decrease in Cy3 spectra appeared greater than the effect on the Cy5 spectra, which could dramatically affect the interpretation of FRET efficiency (Fig. 5*B*). We also noted a modest effect of DMSO on the direct excitation of Cy3-labeled HsMSH2-HsMSH6 and HsMSH2-HsMSH3 (Fig. 5, *C* and *D*). Nevertheless, the overall shape of the Cy3 emission curve appeared largely unchanged suggesting that FRET excitation of a Cy5 fluorophore is achievable.

The studies performed in the presence of 5% DMSO (Fig. 5, *A* and *B*) implied that a direct comparison to FRET values obtained in the presence of a G/C duplex DNA was required to interpret any changes in FRET efficiency. In addition, DMSO concentrations above 1% appeared to decrease the direct excitation of Cy3 enough to significantly reduce the FRET efficiency with Cy5-DNA substrates. Because HsMSH2-

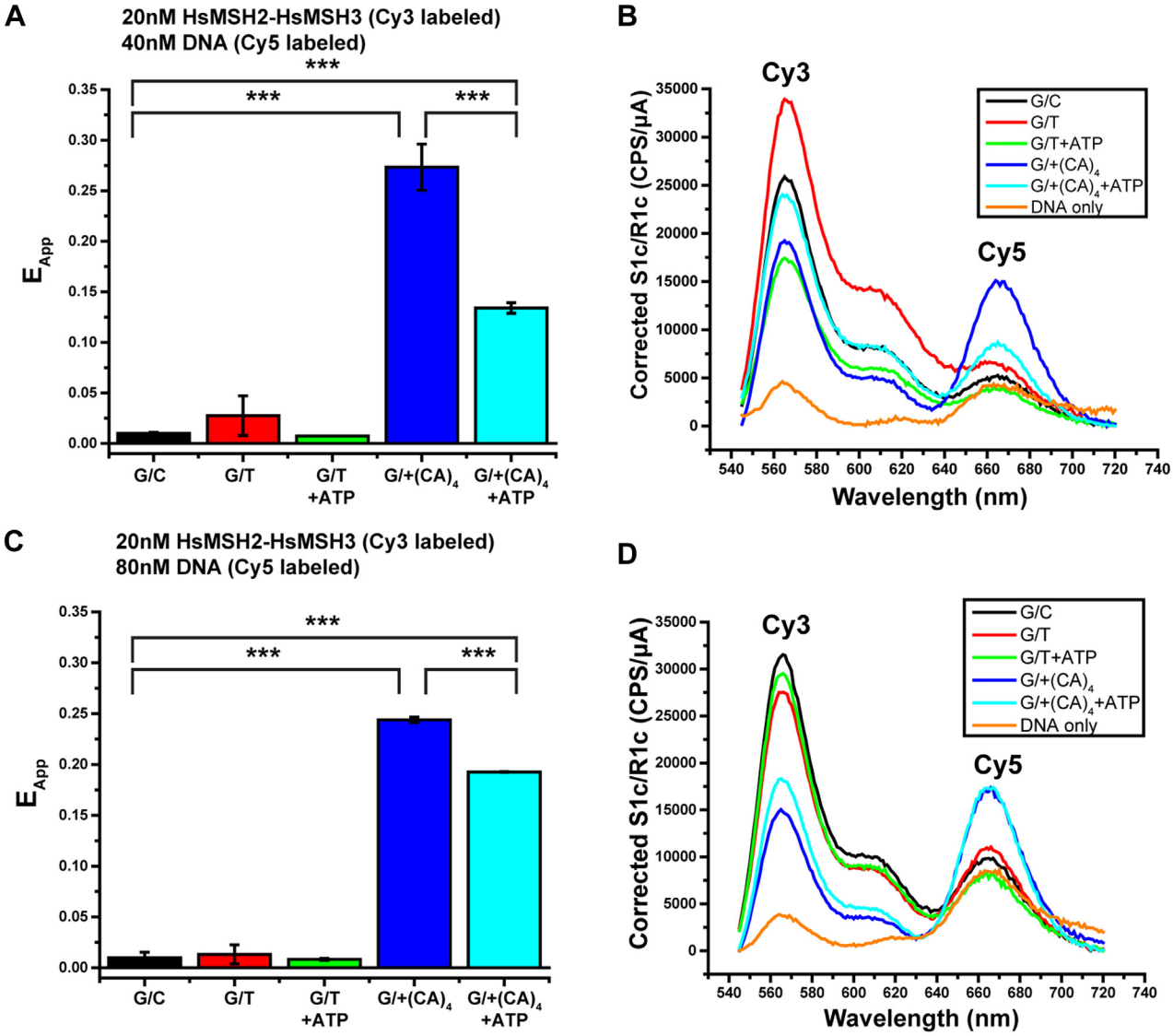

Figure 4. FRET analysis of mismatch recognition by HsMSH2-HsMSH3. *A*, E_{App} bar graph of 1:4 (HsMSH2-HsMSH3:DNA) for G/C; G/T; G/T + ATP; G/+(CA)$_4$; G/+(CA)$_4$ + ATP (mean ± SD). HsMSH2-HsMSH3 does not bind G/C DNA (*black*) and preferentially binds G/+(CA)$_4$ DNA (*red*). HsMSH2-HsMSH3 displays a reduced FRET efficiency upon binding ATP. ***$p < 0.001$, by unpaired *t* test. *B*, representative intensity *versus* wavelength of 1:4 (HsMSH2-HsMSH3:DNA) for G/C; G/T; G/T + ATP; G/+(CA)$_4$; G/+(CA)$_4$ + ATP. *C*, E_{App} bar graph of 1:2 (HsMSH2-HsMSH3:DNA) for G/C; G/T; G/T + ATP; G/+(CA)$_4$; G/+(CA)$_4$ + ATP (mean ± SD). HsMSH2-HsMSH3 does not bind G/C DNA (*black*) and preferentially binds G/(CA)$_4$ DNA (*red*). HsMSH2-HsMSH3 displays a reduced FRET efficiency upon binding ATP. ***$p < 0.001$; by unpaired *t* test. *D*, representative intensity *versus* wavelength of 1:2 (HsMSH2-HsMSH6:DNA) for G/C; G/T; G/T + ATP; G/+(CA)$_4$; G/+(CA)$_4$ + ATP. FRET, Förster resonance energy transfer.

HsMSH6 displayed the lowest FRET efficiency compared to HsMSH2-HsMSH3, we used it as a bellwether to examine the effect of DMSO on the ability to distinguish mismatch binding (elevated FRET) and sliding clamp formation (time-averaged reduced FRET; Fig. 6). The FRET efficiency of G/T-binding by HsMSH2-HsMSH6 decreased by at least 50% as the DMSO concentration was increased to 1% (Fig. 6). Nevertheless, the FRET efficiency of G/T binding (G/T, red bars) remained statistically significant compared to the G/C duplex DNA substrate (G/C, black bars; $p_{40\ nM} = 0.0001$, $p_{80\ nM} = 0.01$). Similarly, the time-averaged FRET efficiency of sliding clamp formation (G/T+ATP, green) decreases with increasing DMSO (Fig. 6). However, we found significant FRET efficiency for sliding clamp formation (G/T+ATP, green bars) compared to G/C duplex (G/C, black bars) below 0.5% DMSO with both 40 nM and 80 nM DNA, while that the FRET efficiency of sliding clamp formation was not significant above the G/C duplex at or above 0.5% DMSO (Fig. 6). These observations suggest that the MSH-DNA FRET-based system may be useful as a compound screening tool when the DMSO concentration is maintained below 0.5%. Perhaps more importantly, it appears that this FRET system may be capable of differentially distinguishing the effects of compounds on HsMSH2-HsMSH6 and HsMSH2-HsMSH3 (discussed below).

Discussion

Decades of studies have clearly determined that MSH proteins recognized mismatched nucleotides and in the presence of ATP form an exceptionally stable sliding clamp on the DNA

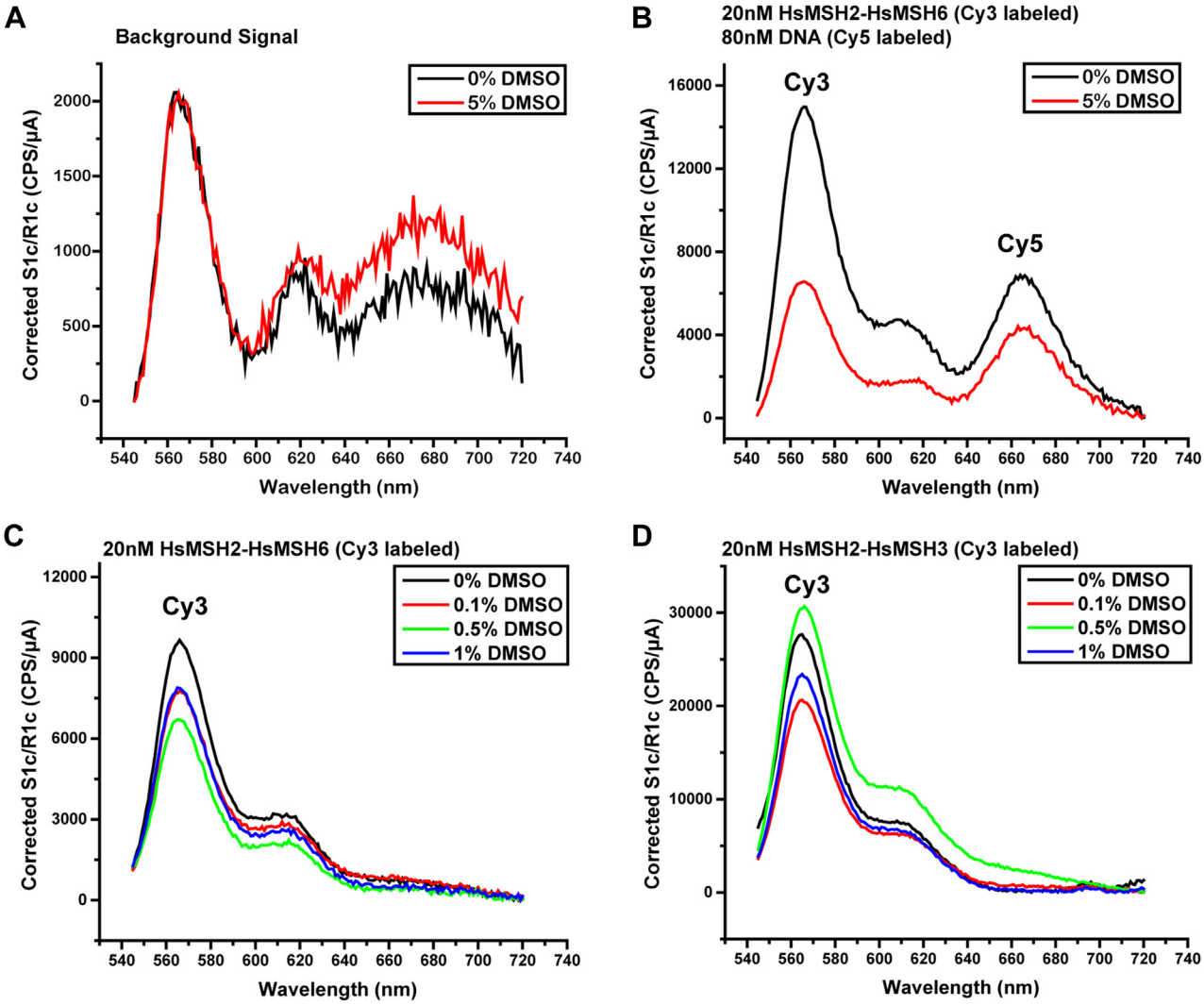

Figure 5. The effect of DMSO on fluorescence excitation and emission. *A*, representative intensity *versus* wavelengths of background signal of DMSO in the absence of fluorophore. No effect is noted in the Cy3 spectra (550–650 nm). An increase in fluorescence is noted in the Cy5 spectra (650–750 nm). *B*, effect of 5% DMSO in the presence of HsMSH2-HsMSH6 (Cy3 labeled) and DNA (Cy5 labeled). A decrease in the Cy3 spectra is observed, while an increase in the Cy5 spectra occurs. This decrease in donor (Cy3) and increase in acceptor (Cy5) will result in a skewed FRET value. *C*, effect of increasing DMSO on HsMSH2-HsMSH6 (Cy3 labeled) signal. *D*, effect of increasing DMSO on HsMSH2-HsMSH3 (Cy3 labeled) signal. DMSO, dimethyl sulfoxide; FRET, Förster resonance energy transfer.

(9, 10, 12–23). This class of proteins includes members that appear principally involved in postreplication MMR as well as exclusive process such as those associated with double strand break repair during meiosis (1, 60). In eukaryotes such as *S. cerevisae* and human cells, it is generally believed that two heterodimeric version, MSH2-MSH3 and MSH2-MSH6, play overlapping and redundant roles in postreplication MMR (1, 61–63). However, it is worth noting that while MSH2-MSH6 appears quite promiscuous on recognizing all the single nucleotide mismatches as well as a variety of small-to-medium IDL mismatches (49, 56, 64), MSH2-MSH3 recognized single nucleotide mismatches poorly and clearly favors small-to-large IDL mismatches (8, 10, 33, 43, 62, 65). Moreover, the cellular concentration of MSH2-MSH3 appears to be at least 10-fold lower than MSH2-MSH6 (44, 66). Finally, no pathogenic mutations of *HsMSH3* have been found that lead to LS/HNPCC, while mutations of the core postreplication MMR genes *HsMSH2*, *HsMSH6*, *HsMLH1*, and *HsPMS2* have been identified as abundant causes of this cancer predisposition.

Using bulk biochemical and single-molecule imaging analysis, we have probed and compared the properties of *E. coli* EcMutS and human HsMSH2-HsMSH3 and HsMSH2-HsMSH6 proteins. All of these MSH proteins display exceptional stability as ATP-bound sliding clamps on DNA. Compared to TaqMutS (10 min), EcMutS (3.25 min) and HsMSH2-HsMSH6 (3.4 min) display a significantly shorter lifetime as sliding clamps on the mismatched DNA (Fig. 2, *C* and *D*). However, it seems likely that the TaqMutS lifetime might be inflated since ATP hydrolysis is required to release MSH sliding clamps from the DNA (12, 20). In this case, TaqMutS is most active at temperatures above 40 °C, while the single-molecule imaging studies that are essential to generate lifetime data were performed at room temperature (∼23 °C). Nevertheless, HsMSH2-HsMSH3 displayed a sliding clamp

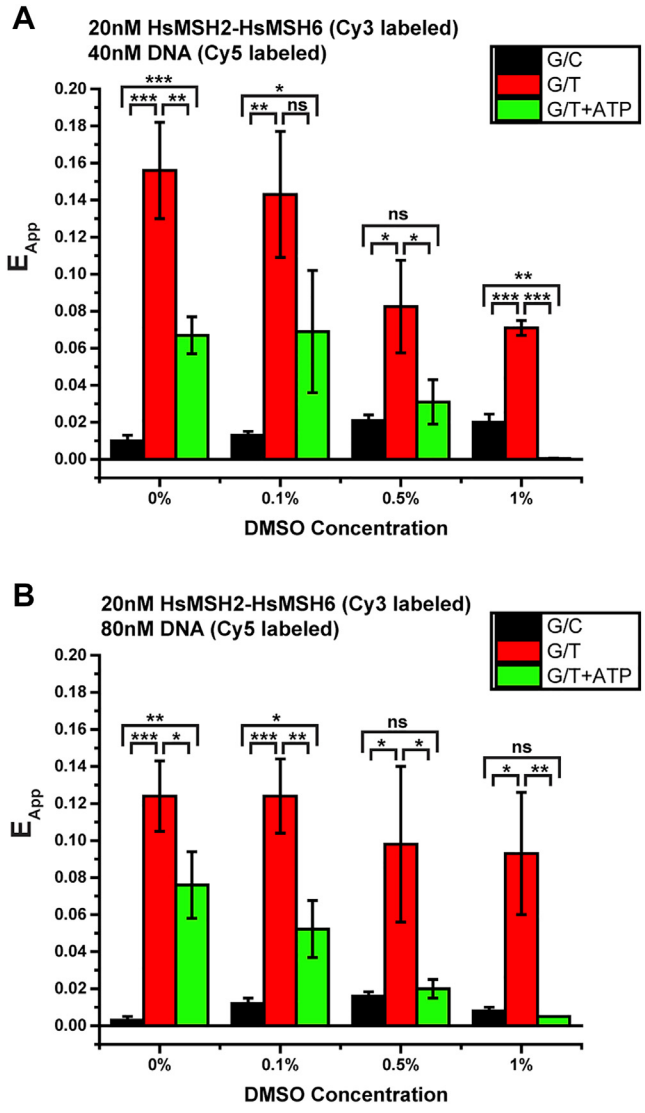

Figure 6. The effect of DMSO on HsMSH2-HsMSH6 FRET. *A*, E_{App} bar graph of 1:2 (HsMSH2-HsMSH6:DNA) for G/C; G/T; G/T + ATP in the presence of DMSO (mean ± SD). At 0.5% DMSO and greater the ability to distinguish between the three states (unbound (G/C), bound to a mismatch (G/T), sliding clamp (G/T + ATP)) is lost. *$p < 0.05$; **$p < 0.01$; ***$p < 0.001$; by unpaired *t* test. *B*, E_{App} bar graph of 1:4 (HsMSH2-HsMSH6:DNA) for G/C; G/T; G/T + ATP in the presence of DMSO (mean ± SD). At 0.5% DMSO and greater the ability to distinguish between the three states (unbound (G/C), bound to a mismatch (G/T), and sliding clamp (G/T + ATP)) is lost. *$p < 0.05$; **$p < 0.01$; ***$p < 0.001$; by unpaired *t* test. DMSO, dimethyl sulfoxide; FRET, Förster resonance energy transfer.

lifetime on the mismatched DNA of 17 min (Fig. 2*E*). Moreover, we note that the single-molecule imaging studies supporting this long lifetime included time points in excess of 60 min, suggesting that HsMSH2-HsMSH3 remains active for an exceedingly long time at room temperature (~23 °C). Such protein stability is important for inhibitory compound screening studies that utilize robotic distribution of components (see below). We note that the lifetime of HsMSH2-HsMSH3 as a sliding clamp on DNA appears to widen the functional differences between it and the core MMR heterodimer HsMSH2-HsMSH6, potentially expanding and/or differentiating the cellular role(s) of HsMSH2-HsMSH3.

A major difference with MSH2-MSH6 is the role of MSH2-MSH3 in TNR expansion that leads to devastating diseases such as Huntington's chorea and myotonic dystrophy (47) While mutation of the core MMR components that include MSH2-MSH6 results in expansions and contractions of short simple repeats (microsatellite instability) (67), deletion of *MSH3* virtually eliminates TNR expansion (68). These apparently opposing expansion-contraction phenotypes on repeat DNA sequences have never been adequately explained. One hypothesis for why *HsMSH3* mutations have not been linked to a cancer phenotype considers the possibility that a defect in HsMSH2-HsMSH3 could lead to substantially more frameshift mutations than defects in HsMSH2-HsMSH6. If true, it is conceivable that the greater number of frameshifts would result in an increased number of abnormal or truncated surface antigens that could stimulate an immune response, resulting in termination of *HsMSH3* mutant cells before a cancer phenotype could be established. Supporting this notion is the observation that PD1 inhibitors that reactivate immune recognition cells are exceedingly effective therapeutic treatments for MMR defective tumors where frameshift mutations remain a minor but highly immunogenic component of the total mutation load (69–71).

Taken as a whole, these observations suggest that the identification of specific inhibitors of HsMSH2-HsMSH3, which have no effect on MSH2-MSH6 activities, might be useful as therapeutics. Inhibition of HsMSH2-HsMSH3 could ameliorate the somatic effects that are generally the most immediately pathological in TNR diseases (72), while preventing the tumorigenesis associated with MMR defects (73). Our studies have reduced to practice a simple FRET-based screen that relies on the remarkably long lifetime and stability of MSH sliding clamps (Figs. 3 and 4). The assay relies on the conversion of mismatch binding events to a stable sliding clamp that continues to exhibit time-averaged FRET (Fig. 3*A*). Since the mismatch affinity for the human MSH proteins appears to engender an ionic strength peak, while sliding clamp formation and lifetime seem to be relatively unaffected by salt, we recommend the reaction buffer for this FRET system to be ~100 mM total ionic strength. We calculated the statistical effect size (z-factor) HTP drug screening comparing a variety of FRET-generating events (Fig. S5) (74, 75). What is most evident from these plots is that FRET events generated by HsMSH2-HsMSH3 provide the largest z-factor margin for the detection of inhibitory events. These calculations suggest that an initial HTP compound screen focused on HsMSH2-HsMSH3 functions could identify specific inhibitors if they exist. This initial screen could then be followed by a counter screen for HsMSH2-HsMSH6 functions to identify specific inhibitors of HsMSH2-HsMSH3 that do not affect HsMSH2-HsMSH6. Because the z-factor for HsMSH2-HsMSH6 functions in significantly lower than HsMSH2-HsMSH3 functions, more redundant FRET repeats will be required to assure statistical significance (Fig. S5). Nevertheless, the stability of the FRET system should be able to easily accommodate the extra duplicates.

Experimental procedures

EcMutS expression, purification, and labeling

EcMutS(D835R,R840E) protein, that is incapable of tetramerization but fully functional for mismatch repair (53), was expressed, purified, and labeled with fluorophore as previously described (76). Briefly, EcMutS was expressed in BL21 AI *Escherichia coli* cells and purified by FPLC using a Ni-NTA column (Qiagen) and Heparin (GE Healthcare) column (26). EcMutS-containing fractions were dialyzed in storage buffer (25 mM Hepes pH 7.8, 1 mM DTT, 0.1 mM EDTA, 150 mM NaCl, 20% glycerol) and frozen at −80 °C.

For fluorophore-labeled proteins, EcMutS and MtFGE (ratio 1:1) were dialyzed together in conversion buffer at 4 °C for 48 h and then dialyzed in labeling buffer overnight. Proteins were then incubated with HIPS-AlexaFluor 647 at 0 °C for 48 h (76). Labeled EcMutS was separated from free dye and MtFGE on a heparin column. Fractions were visualized on an 8% SDS-PAGE and dialyzed in storage buffer (25 mM Hepes pH 7.8, 1 mM DTT, 0.1 mM EDTA, 150 mM NaCl, 20% glycerol) and frozen at −80 °C.

HsMSH2-HsMSH6 expression and purification

Wildtype HsMSH2-MSH6 protein was expressed and purified as previously described (19). Briefly, HsMSH2 and HsMSH6 were coexpressed in Hi5 insect cells using the Bac-to-Bac Baculovirus Expression System (Invitrogen). Protein was purified by FPLC using a Ni-NTA column (Qiagen), PBE-94 column (Sigma), HiLoad 16/60 Superdex 200 (GE Healthcare), and MonoQ 5/50 GL (GE Healthcare). HsMSH2-MSH6 containing fractions were dialyzed in storage buffer (25 mM Hepes pH 7.8, 1 mM DTT, 0.1 mM EDTA, 150 mM NaCl, 20% glycerol) and frozen at −80 °C.

DNA preparation

For surface plasmon resonance DNAs (82-mers) were prepared as follows. Oligonucleotides were synthesized by Integrated DNA Technologies (Table S1). The single-stranded (ss) oligos were purified by PAGE and annealed overnight by step-down cooling in a thermocycler to create double-stranded (ds) oligos. The G-Strand used in every construct contained the biotin moiety that is necessary for surface linkage (Table S1). The complementary T-strand either contained a 5′ digoxigenin (dig) modification or no modification (Table S1) and when annealed to the G-strand created a G/T mismatch. The annealed oligos were purified using a GenPak Fax (Waters) column on an HPLC.

The DNA for smTIRF was prepared as previously described (26). Briefly, a 7-kb fragment of DNA was prepared by digesting a plasmid with *BsaI*. λ-phage DNA (3.2 nM, Thermo Scientific) was ligated with Lambda Mismatch 2A and Lambda Mismatch 2B (800 nM, Table S1) followed by digestion with *BsaI*. The treated λ-DNA was then ligated with the 7-kb DNA, 1000x Lambda Hairpin Linker 1, and Lambda Hairpin Linker 2 (Table S1). The 18.4-kb band was excised and purified utilizing β-agarase, ethanol precipitation, and stored at −80 °C (26).

The DNA for FRET studies were prepared as follows. The 41-mer oligonucleotides for were synthesized by Integrated DNA Technologies and labeled with near 100% efficiency using fluorescent (Cy/AF) dyes. To increase homogeneity between multiple substrates, the G-strand is always labeled with the acceptor fluorophore and then annealed with a complementary strand containing no mismatch (G/C), a single nucleotide mismatch (G/T), or an IDL mismatch [G/+$(CA)_4$].

Single strand DNA containing an amino modifier C6 dT (IDT) in aqueous solution (10 mM Tris-HCl pH 8.0, 1 mM EDTA) was precipitated using 3 M sodium acetate pH 5.2, 95% ethanol, and glycogen, followed by a wash with 70% ethanol to remove any impurities remaining from the synthesis process (Table S1). The precipitate was then air-dried and resuspended in labeling buffer (70–100 μl 0.1 M sodium tetraborate pH 8.5). Cy-dye or analog, dissolved in dimethylformamide and added to the reaction in 10 to 30× molar excess. The reaction was mixed until completely dissolved and kept in foil rotating overnight at 23 °C and 500 rpm. The overnight labeled material was ethanol precipitated following the same protocol as above twice to remove free dye. The final pellet should be fluorescent, and if color is not observed, the labeling should be repeated before subsequent HPLC purification steps. The final pellet was dissolved in triethylamine acetate.

The fluorophore-labeled ssDNA oligonucleotide was separated from unlabeled oligonucleotide and unincorporated free fluorophore by C18 reverse-phase HPLC chromatography (Poroshell 120 EC-C18, Agilent). Labeled fractions were pooled, and ethanol precipitated as described above and resuspended in aqueous solution (10 mM Tris-HCl pH 8.0, 1 mM EDTA).

The fluorophore-labeled G-strand oligonucleotide was annealed with complementary unlabeled DNA (C-strand no mismatch, T-strand single nucleotide mismatch, +$(CA)_4$-strand IDL mismatch) in a 1:1 M ratio by heating to 95 °C and slow step cooling (Table S1). The duplex DNA products were then purified from any remaining ssDNA substrates by ion exchange HPLC chromatography (Gen-Pack Fax, Waters). Duplex fractions were pooled, and ethanol precipitated as described above and resuspended in aqueous solution (10 mM Tris-HCl pH 8.0, 1 mM EDTA).

Preparation of SPR sensor chip

A streptavidin-coated Biacore 3000 SPR sensor chip (Sensor Chip SA, GE Healthcare) containing four channels was preconditioned with NaOH (50 mM). Biotin only and biotin-digoxigenin dsDNA (described above) was immobilized on the chip, with dsG/T-dig (blocked-end) DNA in channel 2 and dsG/T (open-end) DNA in channel 4, leaving channels 1 and 3 as buffer-only reference channels. The SPR response units (RUs) were kept within 10 between channels 2 and 4 to ensure the similar amounts of DNA was immobilized in each channel.

SPR experimental setup

Experiments were performed at 25 °C. EcMutS and HsMSH2-MSH6 were examined independently using the same

chip. A preblocking of the dig with anti-digoxigenin (anti-dig, 50 nM, Roche) was performed prior to each experiment. While no change in SPR RUs was noted, previous work has shown that the anti-digoxigenin is enough to block/trap MSH clamps on the DNA (19, 20, 77). The running buffer for both proteins was 25 mM Hepes pH 7.8, 0.1 mM DTT, 0.1 mM EDTA, 10 mM $MgCl_2$, 200 μg/ml acetylated BSA (Promega), 0.01% P-20 surfactant (GE Healthcare), 1 nM anti-dig (Roche), and stated [NaCl]. Proteins were diluted prior to experiment to reduce glycerol and adjust NaCl concentrations. Injections containing no protein were performed at the beginning and end of the analysis to ensure that background binding was unchanged between analysis.

For ionic strength binding/stability analysis, a titration of EcMutS and HsMSH2-MSH6 (0–100 nM) was first performed to determine the protein concentration that reflected ∼80% binding saturation (Figs. S1 and S2). The experimental concentration of 40 nM MSH proteins for ionic strength binding/stability analysis was chosen. Ionic binding experiments consisted of ten NaCl conditions 15, 30, 60, 80, 100, 120, 140, 160, and 180 mM NaCl. When ionic strength is referred to it is only that of NaCl. RU changes reflect the binding and dissociation over time. ATP-induced dissociation was tested with an addition of running buffer containing ATP (1 mM, Roche) following binding of the MSH homolog. Following the ATP injection, the surface was regenerated with 1 M NaCl to remove any remaining protein while leaving the DNA undamaged. Injections containing no protein were performed at the beginning and end of the analysis to ensure that background binding was unchanged between analysis.

SPR analysis of MSH activity

The SPR flow scheme is outlined in Figs. S1 and S2. Briefly, the MSH protein was injected to monitor binding followed by a buffer wash step that monitored dissociation. The binding-dissociation was followed by injection of binding-dissociation buffer containing ATP that results in a transition to an MSH sliding clamp that rapidly dissociated from the open end of an unblocked mismatched DNA (Figs. S1*B* and S2*B*). In contrast, blocked-end mismatched DNA retains the MSH sliding clamps that exhibit a dissociation rate which reflects intrinsic stability (Figs. S1*A* and S2*A*).

Raw RUs were collected for each independent channel (1–4). Subtractions of the empty reference channels (2-1, 4-3) was performed to account for nonspecific adsorption of protein to the surface. This subtraction data were used for all analysis. Runs were performed in triplicate. SPR analysis was performed using MATLAB software. For each salt concentration, response data over all three replicates were globally fit to a 1:1 interaction model with a parameter for mass transport. Specifically, the k_{on} and k_{off} parameters were fit during the MSH binding, the k_{off} was simultaneously fit during the buffer wash, and the k_{off} and $k_{off\bullet ATP}$ were fit during the ATP wash. Fitting the ATP wash of the open-ended DNA responses left a considerable residual. However, this residual was largely constant over time during the ATP wash indicating the fast disassociation with ATP was accurately captured by the model.

Preparation of smTIRF flow cell

A laboratory engineered flow cell was used for all experiments consisting of a neutravidin-coated, PEG passivated quartz slide surface. Laminar flow (250 μl/min) was used to inject and stretch the biotinylated dsDNA (as described above, 300 pM) in 300 μl T-50 buffer (20 mM Tris-HCL, pH 7.5, 50 mM NaCl) on the surface. Prior to performing an experiment, the flow cells and all relevant tubing were prepared with BSA and P-20 to prevent nonspecific adsorption that may reduce concentrations.

smTIRF experiments and data analysis

Single-molecule fluorescence data were attained on a home-built prism-type TIRF microscope (26) with green (532 nm) and red (635 nm) laser lines. Emissions were split by a Dual View optical setup (DV2, Photometrics) in bypass mode before collection using an EMCCD camera (ProEM Exelon512, Princeton Instruments). Laser excitation was modulated by the opening and closing of shutter controlled by Micro-Manager image capture software (78).

The single-molecule imaging buffer was 20 mM Tris-HCl (pH 7.5), 5 mM $MgCl_2$, 0.1 mM DTT, 200 μg/ml acetylated BSA (Promega), 0.0025% P-20 surfactant (GE Healthcare), 1 mM ATP (Roche), and stated [NaCl]. The imaging buffer included saturated (∼3 mM) Trolox, PCA (1 mM), and PCD (10 nM) to minimize photo blinking and photobleaching (79, 80).

EcMutS lifetime was calculated by flowing AF647-EcMutS (5 nM) into the prepared flow cell. In the absence of flow protein–DNA interactions were observed live. After recording Syto 59 (1000 nM, Invitrogen) was used to stain the DNA. At least two laser power settings were examined to clearly distinguish lifetime-dependent dissociation from fluorophore photobleaching. Reported lifetimes varied less than 10% at two laser power settings.

Preparation of the Cy3-peptide

Ten milligram of lyophilized peptide containing a Sortase recognition sequence (81, 82) and a single cystine residue for maleimide labeling (CLPETGG, GenScript) was dissolved in reaction buffer (50 mM Tris 7.0 and 5 mM TCEP) and incubated at room temperature for 30 min. The reaction was then added to 3 mg of lyophilized Sulfo-Cy3 maleimide (Lumiprobe) and incubated overnight at 4 °C. The labeled peptide was purified with reverse-phase HPLC chromatography (Zorbax SB-C18, Agilent). Peak fractions were lyophilized and stored at −80 °C until needed. For labeling, the peptide was dissolved in Sortase reaction buffer (25 mM Hepes pH 7.8, 150 mM NaCl, and 10% glycerol).

MSH Sortase-tag addition, expression, purification, and labeling

MSH proteins may be modified on the N terminus to contain a hexa-histidine (his_6), two serine spacers, a Sortase recognition sequence, and a flexible linker (GGGS) attached to the MSH protein of interest. For these studies, the tags were placed on HsMSH6 and HsMSH3. MSH proteins were cloned into pFastBac1 (Invitrogen). The heterodimeric proteins (HsMSH2-HsMSH6, HsMSH2-HsMSH3) were coexpressed as previously described (10, 16) in Sf9 cells using the Bac-to-Bac Baculovirus Expression System (Invitrogen). Protein was first purified by FPLC using a Ni-NTA column (Qiagen) followed by a heparin column (GE Healthcare). Peak fractions were pooled and combined with four-times molar ratio of the Sortase protein and 50-times molar ratio of the Cy3-Peptide for 30 min at 4 °C (82, 83). The reaction is quenched with 20 mM EDTA and loaded onto a spin-desalting column (40K Zeba Spin Desalting Column, Thermo Scientific). The eluent was then separated from the Cy3-peptide using a second heparin column (GE Healthcare) and polished using a MonoQ 5/50 GL (GE Healthcare). The HsMSH2-HsMSH6 and HsMSH2-HsMSH3 containing fractions were dialyzed in storage buffer (25 mM Hepes pH 7.8, 1 mM DTT, 0.1 mM EDTA, 150 mM NaCl, 20% glycerol) and frozen at −80 °C.

FRET mismatch recognition assay analysis

FRET detection was performed utilizing a FlouroMax-4 (Horiba Jobin Yvon) according to manufacturer's recommendations (84). The Flouromax-4 (Horiba Jobin Yvon) is a corrected photon counting system where the Intensity (counts per second/μA) is corrected signal detector (S1c)/corrected reference detector (R1c) or S1c/R1c. Because FRET calculations are ratios of acceptor and donor intensities, the S1c/R1c read-out from the FluoroMax (or any other corrected photon counting reader) may be used directly as measures of fluorescence intensity (I). While peak intensity at specific donor (∼560 nm) and acceptor (∼670 nm) wavelengths may be used as an initial screen for FRET efficiency calculations, increased accuracy is obtained by fitting the entire scanned peak intensities to a Gaussian function and integrating. Apparent FRET efficiency (E_{App}) is calculated by: $E_{App} = (I_A - I_{A•DNA\ Only})/[(I_A - I_{A•DNA\ Only}) + (I_D - I_{D•DNA\ Only})]$, where I_A is the MSH+DNA acceptor intensity, $I_{A•DNA\ Only}$ is the acceptor intensity of the DNA alone, I_D is the donor intensity, and $I_{D•DNA\ Only}$ is the donor intensity of the DNA alone. Thus, E_{App} corrects for background contribution of 510 nm excitation that results in the acceptor Cy5-DNA Gaussian emissions with peaks at ∼560 nm and at ∼670 nm in the absence of donor Cy3-MSH protein. The donor Cy3-MSH protein alone does not contribute to background Gaussian emission with a peak at ∼670 nm and therefore does not require a correction factor.

The biotin-labeled DNA was preblocked with a 1:2 M ratio of NeutrAvidin (ThermoFisher) immediately prior to the experiment. The reaction buffer for both proteins was 25 mM Hepes pH 7.8, 100 mM NaCl, 0.1 mM DTT, 0.1 mM EDTA, 10 mM $MgCl_2$, 200 μg/ml acetylated BSA (Promega). ATP (1 mM, Roche) was added where indicated.

The emission spectra was scanned from 545 nm to 720 nm following 510 nm excitation with a xenon lamp. The Cy3 peak was fit with 2 Gaussian functions due to the emission spectra of Cy3. The Cy5 emission peak was fit with a single Gaussian function. The E_{App} FRET was calculated by measuring energy transfer under donor/acceptor intensity ratio (ratiometric FRET). A Cy5-labeled 41-bp duplex DNA containing a G/C duplex, G/T mismatch, or $+(CA)_4$ IDL mismatch with 3′ biotin on both strands was end blocked with neutravidin was used. Cy3-labeled MSH protein was kept constant at 20 nM. The molar ratio was varied by increasing and decreasing the amount of DNA. Experiments were performed in a quartz cuvette on a FlouroMax-4 (Horiba Jobin Yvon) 5 min following the addition of protein. The addition of 1 mM ATP was tested. Binding of MSH protein to the mismatch should result in a high FRET value (Fig. 3, top). The addition of ATP should result in a sliding clamp that results in a time-averaged FRET (Fig. 3, bottom). As the ratio of donor to acceptor is increased a higher FRET value is observed.

Data availability

All raw and processed data contained in the manuscript are available from the corresponding author upon request.

Supporting information—This article contains supporting information.

Acknowledgments—We would like to thank members of the Fishel laboratory for insights and helpful discussions.

Author contributions—B. M. B., J.-B. L., and R. F. methodology; B. M. B., J. L., J. M.-L., and J. A. L. investigation; B. M. B., N. D. J., J.-B. L., and R. F. formal analysis; B. M. B., J.-B. L., and R. F. writing-original draft.

Funding and additional information—This work was supported by National Institutes of Health grants CA067007 and GM129764 (R. F.) and the Global Research Lab Program through the NRF of Korea funded by the Ministry of Science and ICT 2017K1A1A2013241 (J.-B. L.). The content is solely the responsibility of the authors and does not necessarily represent the official views of the National Institutes of Health.

Conflict of interest—The authors declare no conflicts of interest with the contents of this article.

Abbreviations—The abbreviations used are: DMSO, dimethyl sulfoxide; Ec, *E. coli*; FRET, Förster resonance energy transfer; HTP, high-throughput; IDL, insertion-deletion loop-type; LS/HNPCC, Lynch syndrome or hereditary nonpolyposis colorectal cancer; MLH/PMS, MutL homolog; MMR, mismatch repair; MSH, MutS homolog; smTIRF, single-molecule total internal reflection fluorescence; SPR, surface plasmon resonance; TNR, trinucleotide repeat.

References

1. Fishel, R. (2015) Mismatch repair. *J. Biol. Chem.* **290**, 26395–26403
2. Fishel, R. A., Siegel, E. C., and Kolodner, R. (1986) Gene conversion in Escherichia coli. Resolution of heteroallelic mismatched nucleotides by co-repair. *J. Mol. Biol.* **188**, 147–157
3. Su, S.-S., and Modrich, P. (1986) Escherichia coli mutS-encoded protein binds to mismatched DNA base pairs. *Proc. Natl. Acad. Sci. U. S. A.* **83**, 5057–5061
4. Kolodner, R. D., Mendillo, M. L., and Putnam, C. D. (2007) Coupling distant sites in DNA during DNA mismatch repair. *Proc. Natl. Acad. Sci. U. S. A.* **104**, 12953–12954
5. Ortega, J., Lee, G. S., Gu, L., Yang, W., and Li, G. M. (2021) Mispair-bound human MutS-MutL complex triggers DNA incisions and activates mismatch repair. *Cell Res.* **31**, 542–553
6. Qiu, R., Sakato, M., Sacho, E. J., Wilkins, H., Zhang, X., Modrich, P., *et al.* (2015) MutL traps MutS at a DNA mismatch. *Proc. Natl. Acad. Sci. U. S. A.* **112**, 10914–10919
7. Walker, J. E., Saraste, M., Runswick, M. J., and Gay, N. J. (1982) Distantly related sequences in the alpha-and beta-subunits of ATP synthase, myosin, kinases and other ATP-requiring enzymes and a common nucleotide binding fold. *EMBO J.* **1**, 945–951
8. Palombo, F., Iaccarino, I., Nakajima, E., Ikejima, M., Shimada, T., and Jiricny, J. (1996) hMutSbeta, a heterodimer of hMSH2 and hMSH3, binds to insertion/deletion loops in DNA. *Curr. Biol.* **6**, 1181–1184
9. Snowden, T., Acharya, S., Butz, C., Berardini, M., and Fishel, R. (2004) hMSH4-hMSH5 recognizes Holliday Junctions and forms a meiosis-specific sliding clamp that embraces homologous chromosomes. *Mol. Cell* **15**, 437–451
10. Wilson, T., Guerrette, S., and Fishel, R. (1999) Dissociation of mismatch recognition and ATPase activity by hMSH2-hMSH3. *J. Biol. Chem.* **274**, 21659–21664
11. Gorman, J., Wang, F., Redding, S., Plys, A. J., Fazio, T., Wind, S., *et al.* (2012) Single-molecule imaging reveals target-search mechanisms during DNA mismatch repair. *Proc. Natl. Acad. Sci. U. S. A.* **109**, E3074–E3083
12. Jeong, C., Cho, W. K., Song, K. M., Cook, C., Yoon, T. Y., Ban, C., *et al.* (2011) MutS switches between two fundamentally distinct clamps during mismatch repair. *Nat. Struct. Mol. Biol.* **18**, 379–385
13. Acharya, S., Foster, P. L., Brooks, P., and Fishel, R. (2003) The coordinated functions of the E. coli MutS and MutL proteins in mismatch repair. *Mol. Cell* **12**, 233–246
14. Cho, W. K., Jeong, C., Kim, D., Chang, M., Song, K. M., Hanne, J., *et al.* (2012) ATP alters the diffusion mechanics of MutS on mismatched DNA. *Structure* **20**, 1264–1274
15. Gradia, S., Acharya, S., and Fishel, R. (1997) The human mismatch recognition complex hMSH2-hMSH6 functions as a novel molecular switch. *Cell* **91**, 995–1005
16. Gradia, S., Subramanian, D., Wilson, T., Acharya, S., Makhov, A., Griffith, J., *et al.* (1999) hMSH2-hMSH6 forms a hydrolysis-independent sliding clamp on mismatched DNA. *Mol. Cell* **3**, 255–261
17. Hargreaves, V. V., Shell, S. S., Mazur, D. J., Hess, M. T., and Kolodner, R. D. (2010) Interaction between the Msh2 and Msh6 nucleotide-binding sites in the Saccharomyces cerevisiae Msh2-Msh6 complex. *J. Biol. Chem.* **285**, 9301–9310
18. Hargreaves, V. V., Putnam, C. D., and Kolodner, R. D. (2012) Engineered disulfide-forming amino acid substitutions interfere with a conformational change in the mismatch recognition complex Msh2-Msh6 required for mismatch repair. *J. Biol. Chem.* **287**, 41232–41244
19. Heinen, C. D., Cyr, J. L., Cook, C., Punja, N., Sakato, M., Forties, R. A., *et al.* (2011) Human MSH2 (hMSH2) protein controls ATP processing by hMSH2-hMSH6. *J. Biol. Chem.* **286**, 40287–40295
20. Heinen, C. D., Wilson, T., Mazurek, A., Berardini, M., Butz, C., and Fishel, R. (2002) HNPCC mutations in hMSH2 result in reduced hMSH2-hMSH6 molecular switch functions. *Cancer Cell* **1**, 469–478
21. Jiang, J., Bai, L., Surtees, J. A., Gemici, Z., Wang, M. D., and Alani, E. (2005) Detection of high-affinity and sliding clamp modes for MSH2-MSH6 by single-molecule unzipping force analysis. *Mol. Cell* **20**, 771–781
22. Mazur, D. J., Mendillo, M. L., and Kolodner, R. D. (2006) Inhibition of Msh6 ATPase activity by mispaired DNA induces a Msh2(ATP)-Msh6(ATP) state capable of hydrolysis-independent movement along DNA. *Mol. Cell* **22**, 39–49
23. Mendillo, M. L., Mazur, D. J., and Kolodner, R. D. (2005) Analysis of the interaction between the Saccharomyces cerevisiae MSH2-MSH6 and MLH1-PMS1 complexes with DNA using a reversible DNA end-blocking system. *J. Biol. Chem.* **280**, 22245–22257
24. Fernandez-Leiro, R., Bhairosing-Kok, D., Kunetsky, V., Laffeber, C., Winterwerp, H. H., Groothuizen, F., *et al.* (2021) The selection process of licensing a DNA mismatch for repair. *Nat. Struct. Mol. Biol.* **28**, 373–381
25. Groothuizen, F. S., Winkler, I., Cristovao, M., Fish, A., Winterwerp, H. H., Reumer, A., *et al.* (2015) MutS/MutL crystal structure reveals that the MutS sliding clamp loads MutL onto DNA. *Elife* **4**, e06744
26. Liu, J., Hanne, J., Britton, B. M., Bennett, J., Kim, D., Lee, J. B., *et al.* (2016) Cascading MutS and MutL sliding clamps control DNA diffusion to activate mismatch repair. *Nature* **539**, 583–587
27. Liu, J., Lee, R., Britton, B. M., London, J. A., Yang, K., Hanne, J., *et al.* (2019) MutL sliding clamps coordinate exonuclease-independent Escherichia coli mismatch repair. *Nat. Commun.* **10**, 5294
28. London, J., Martin-Lopez, J., Yang, I., Liu, J., Lee, J. B., and Fishel, R. (2021) Linker domain function predicts pathogenic MLH1 missense variants. *Proc. Natl. Acad. Sci. U. S. A.* **118**, e2019215118
29. Hermans, N., Laffeber, C., Cristovao, M., Artola-Boran, M., Mardenborough, Y., Ikpa, P., *et al.* (2016) Dual daughter strand incision is processive and increases the efficiency of DNA mismatch repair. *Nucleic Acids Res.* **44**, 6770–6786
30. Mardenborough, Y. S. N., Nitsenko, K., Laffeber, C., Duboc, C., Sahin, E., Quessada-Vial, A., *et al.* (2019) The unstructured linker arms of MutL enable GATC site incision beyond roadblocks during initiation of DNA mismatch repair. *Nucleic Acids Res.* **47**, 11667–11680
31. Bowen, N., and Kolodner, R. D. (2017) Reconstitution of Saccharomyces cerevisiae DNA polymerase epsilon-dependent mismatch repair with purified proteins. *Proc. Natl. Acad. Sci. U. S. A.* **114**, 3607–3612
32. Smith, C. E., Bowen, N., Graham, W. J. T., Goellner, E. M., Srivatsan, A., and Kolodner, R. D. (2015) Activation of Saccharomyces cerevisiae Mlh1-Pms1 endonuclease in a reconstituted mismatch repair system. *J. Biol. Chem.* **290**, 21580–21590
33. Srivatsan, A., Bowen, N., and Kolodner, R. D. (2014) Mispair-specific recruitment of the Mlh1-Pms1 complex identifies repair substrates of the Saccharomyces cerevisiae Msh2-Msh3 complex. *J. Biol. Chem.* **289**, 9352–9364
34. Kolodner, R. D. (1995) Mismatch repair: mechanisms and relationship to cancer susceptibility. *Trends Biochem. Sci.* **20**, 397–401
35. Kolodner, R. D. (2016) A personal historical view of DNA mismatch repair with an emphasis on eukaryotic DNA mismatch repair. *DNA Repair (Amst.)* **38**, 3–13
36. Lynch, H. T., and de la Chapelle, A. (2003) Hereditary colorectal cancer. *N. Engl. J. Med.* **348**, 919–932
37. Lynch, H. T., and Lynch, J. F. (1993) The Lynch syndromes. *Curr. Opin. Oncol.* **5**, 687–696
38. Lynch, H. T., Snyder, C. L., Shaw, T. G., Heinen, C. D., and Hitchins, M. P. (2015) Milestones of Lynch syndrome: 1895-2015. *Nat. Rev. Cancer* **15**, 181–194
39. Fishel, R., and Heinen, C. D. (2016) Enhanced gene targeting to evaluate Lynch syndrome alterations. *Proc. Natl. Acad. Sci. U. S. A.* **113**, 3918–3920
40. Rath, A., Mishra, A., Ferreira, V. D., Hu, C., Omerza, G., Kelly, K., *et al.* (2019) Functional interrogation of Lynch syndrome-associated MSH2 missense variants via CRISPR-Cas9 gene editing in human embryonic stem cells. *Hum. Mutat.* **40**, 2044–2056
41. Thompson, B. A., Spurdle, A. B., Plazzer, J. P., Greenblatt, M. S., Akagi, K., Al-Mulla, F., *et al.* (2014) Application of a 5-tiered scheme for standardized classification of 2,360 unique mismatch repair gene variants in the InSiGHT locus-specific database. *Nat. Genet.* **46**, 107–115
42. Acharya, S., Wilson, T., Gradia, S., Kane, M. F., Guerrette, S., Marsischky, G. T., *et al.* (1996) hMSH2 forms specific mispair-binding

complexes with hMSH3 and hMSH6. *Proc. Natl. Acad. Sci. U. S. A.* **93**, 13629–13634
43. Dowen, J. M., Putnam, C. D., and Kolodner, R. D. (2010) Functional studies and homology modeling of Msh2-Msh3 predict that mispair recognition involves DNA bending and strand separation. *Mol. Cell. Biol.* **30**, 3321–3328
44. Charbonneau, N., Amunugama, R., Schmutte, C., Yoder, K., and Fishel, R. (2009) Evidence that hMLH3 functions primarily in meiosis and in hMSH2-hMSH3 mismatch repair. *Cancer Biol. Ther.* **8**, 1411–1420
45. Huang, J., Kuismanen, S. A., Liu, T., Chadwick, R. B., Johnson, C. K., Stevens, M. W., *et al.* (2001) MSH6 and MSH3 are rarely involved in genetic predisposition to nonpolypotic colon cancer. *Cancer Res.* **61**, 1619–1623
46. Watanabe, T., Muto, T., Sawada, T., and Miyaki, M. (1996) Flat adenoma as a precursor of colorectal carcinoma in hereditary nonpolyposis colorectal carcinoma [published erratum appears in Cancer 1996 Jun 15;77(12):2646]. *Cancer* **77**, 627–634
47. Jones, L., Houlden, H., and Tabrizi, S. J. (2017) DNA repair in the trinucleotide repeat disorders. *Lancet Neurol.* **16**, 88–96
48. Blackwell, L. J., Bjornson, K. P., and Modrich, P. (1998) DNA-dependent activation of the hMutS alpha ATPase. *J. Biol. Chem.* **273**, 32049–32054
49. Gradia, S., Acharya, S., and Fishel, R. (2000) The role of mismatched nucleotides in activating the hMSH2-hMSH6 molecular switch. *J. Biol. Chem.* **275**, 3922–3930
50. Drummond, J. T., Li, G. M., Longley, M. J., and Modrich, P. (1995) Isolation of an hMSH2-p160 heterodimer that restores DNA mismatch repair to tumor cells. *Science* **268**, 1909–1912
51. Marsischky, G. T., and Kolodner, R. D. (1999) Biochemical characterization of the interaction between the Saccharomyces cerevisiae MSH2-MSH6 complex and mispaired bases in DNA. *J. Biol. Chem.* **274**, 26668–26682
52. Iaccarino, I., Marra, G., Palombo, F., and Jiricny, J. (1998) hMSH2 and hMSH6 play distinct roles in mismatch binding and contribute differently to the ATPase activity of hMutSalpha. *EMBO J.* **17**, 2677–2686
53. Mendillo, M. L., Putnam, C. D., and Kolodner, R. D. (2007) Escherichia coli MutS tetramerization domain structure reveals that stable dimers but not tetramers are essential for DNA mismatch repair *in vivo*. *J. Biol. Chem.* **282**, 16345–16354
54. Blackwell, L. J., Bjornson, K. P., Allen, D. J., and Modrich, P. (2001) Distinct MutS DNA-binding modes that are differentially modulated by ATP binding and hydrolysis. *J. Biol. Chem.* **276**, 34339–34347
55. Blackwell, L. J., Martik, D., Bjornson, K. P., Bjornson, E. S., and Modrich, P. (1998) Nucleotide-promoted release of hMutS alpha from heteroduplex DNA is consistent with an ATP-dependent translocation mechanism. *J. Biol. Chem.* **273**, 32055–32062
56. Marsischky, G. T., Filosi, N., Kane, M. F., and Kolodner, R. (1996) Redundancy of Saccharomyces cerevisiae MSH3 and MSH6 in MSH2-dependent mismatch repair. *Genes Dev.* **10**, 407–420
57. Graham, W. J.t., Putnam, C. D., and Kolodner, R. D. (2018) The properties of Msh2-Msh6 ATP binding mutants suggest a signal amplification mechanism in DNA mismatch repair. *J. Biol. Chem.* **293**, 18055–18070
58. Balakin, K. V., Savchuk, N. P., and Tetko, I. V. (2006) In silico approaches to prediction of aqueous and DMSO solubility of drug-like compounds: trends, problems and solutions. *Curr. Med. Chem.* **13**, 223–241
59. Ilouga, P. E., Winkler, D., Kirchhoff, C., Schierholz, B., and Wölcke, J. (2007) Investigation of 3 industry-wide applied storage conditions for compound libraries. *J. Biomol. Screen.* **12**, 21–32
60. Spies, M., and Fishel, R. (2015) Mismatch repair during homologous and homeologous recombination. *Cold Spring Harb. Perspect. Biol.* **7**, 269–290
61. Jiricny, J. (2006) The multifaceted mismatch-repair system. *Nat. Rev. Mol. Cell Biol.* **7**, 335–346
62. Kolodner, R. D., and Marsischky, G. T. (1999) Eukaryotic DNA mismatch repair. *Curr. Opin. Genet. Dev.* **9**, 89–96
63. Modrich, P. (1997) Strand-specific mismatch repair in mammalian cells. *J. Biol. Chem.* **272**, 24727–24730
64. Mazurek, A., Johnson, C. N., Germann, M. W., and Fishel, R. (2009) Sequence context effect for hMSH2-hMSH6 mismatch-dependent activation. *Proc. Natl. Acad. Sci. U. S. A.* **106**, 4177–4182
65. Harrington, J. M., and Kolodner, R. D. (2007) Saccharomyces cerevisiae Msh2-Msh3 acts in repair of base-base mispairs. *Mol. Cell. Biol.* **27**, 6546–6554
66. Marra, G., Iaccarino, I., Lettieri, T., Roscilli, G., Delmastro, P., and Jiricny, J. (1998) Mismatch repair deficiency associated with overexpression of the MSH3 gene. *Proc. Natl. Acad. Sci. U. S. A.* **95**, 8568–8573
67. Martinez, J. S., von Nicolai, C., Kim, T., Ehlen, A., Mazin, A. V., Kowalczykowski, S. C., *et al.* (2016) BRCA2 regulates DMC1-mediated recombination through the BRC repeats. *Proc. Natl. Acad. Sci. U. S. A.* **113**, 3515–3520
68. van den Broek, W. J., Nelen, M. R., Wansink, D. G., Coerwinkel, M. M., te Riele, H., Groenen, P. J., *et al.* (2002) Somatic expansion behaviour of the (CTG)n repeat in myotonic dystrophy knock-in mice is differentially affected by Msh3 and Msh6 mismatch-repair proteins. *Hum. Mol. Genet.* **11**, 191–198
69. Le, D. T., Durham, J. N., Smith, K. N., Wang, H., Bartlett, B. R., Aulakh, L. K., *et al.* (2017) Mismatch repair deficiency predicts response of solid tumors to PD-1 blockade. *Science* **357**, 409–413
70. Le, D. T., Uram, J. N., Wang, H., Bartlett, B. R., Kemberling, H., Eyring, A. D., *et al.* (2015) PD-1 blockade in tumors with mismatch-repair deficiency. *N. Engl. J. Med.* **372**, 2509–2520
71. Topalian, S. L., Drake, C. G., and Pardoll, D. M. (2015) Immune checkpoint blockade: a common denominator approach to cancer therapy. *Cancer Cell* **27**, 450–461
72. Kennedy, L., Evans, E., Chen, C. M., Craven, L., Detloff, P. J., Ennis, M., *et al.* (2003) Dramatic tissue-specific mutation length increases are an early molecular event in Huntington disease pathogenesis. *Hum. Mol. Genet.* **12**, 3359–3367
73. Kolodner, R. D. (2000) Guarding against mutation. *Nature* **407**, 687–689
74. Sui, Y., and Wu, Z. (2007) Alternative statistical parameter for high-throughput screening assay quality assessment. *J. Biomol. Screen.* **12**, 229–234
75. Zhang, J. H., Chung, T. D., and Oldenburg, K. R. (1999) A simple statistical parameter for use in evaluation and validation of high throughput screening assays. *J. Biomol. Screen.* **4**, 67–73
76. Liu, J., Hanne, J., Britton, B. M., Shoffner, M., Albers, A. E., Bennett, J., *et al.* (2015) An efficient site-specific method for irreversible covalent labeling of proteins with a fluorophore. *Sci. Rep.* **5**, 16883
77. Hanne, J., Britton, B. M., Park, J., Liu, J., Martin-Lopez, J., Jones, N., *et al.* (2018) MutS homolog sliding clamps shield the DNA from binding proteins. *J. Biol. Chem.* **293**, 14285–14294
78. Edelstein, A., Amodaj, N., Hoover, K., Vale, R., and Stuurman, N. (2010) Computer control of microscopes using microManager. *Curr. Protoc. Mol. Biol.* Chapter 14, Unit14 20
79. Senavirathne, G., Liu, J., Lopez, M. A., Jr., Hanne, J., Martin-Lopez, J., Lee, J. B., *et al.* (2015) Widespread nuclease contamination in commonly used oxygen-scavenging systems. *Nat. Methods* **12**, 901–902
80. Senavirathne, G., Lopez, M. A., Jr., Messer, R., Fishel, R., and Yoder, K. E. (2018) Expression and purification of nuclease-free protocatechuate 3,4-dioxygenase for prolonged single-molecule fluorescence imaging. *Anal. Biochem.* **556**, 78–84
81. Dorr, B. M., Ham, H. O., An, C., Chaikof, E. L., and Liu, D. R. (2014) Reprogramming the specificity of sortase enzymes. *Proc. Natl. Acad. Sci. U. S. A.* **111**, 13343–13348
82. Popp, M. W., Antos, J. M., and Ploegh, H. L. (2009) Site-specific protein labeling via sortase-mediated transpeptidation. *Curr. Protoc. Protein Sci.* Chapter 15, Unit 15.13
83. Antos, J. M., Chew, G. L., Guimaraes, C. P., Yoder, N. C., Grotenbreg, G. M., Popp, M. W., *et al.* (2009) Site-specific N- and C-terminal labeling of a single polypeptide using sortases of different specificity. *J. Am. Chem. Soc.* **131**, 10800–10801
84. Melhuish, W. H. (1972) Absolute spectrofluorometry. *J. Res. Natl. Bur. Stand A. Phys. Chem.* **76A**, 547–560